J Mol Neurosci (2015) 57:219–230
DOI 10.1007/s12031-015-0609-3

# RIP1 Inhibition Rescues from LPS-Induced RIP3-Mediated Programmed Cell Death, Distributed Energy Metabolism and Spatial Memory Impairment

Sara Nikseresht[1] · Fariba Khodagholi[1] · Mohsen Nategh[1] · Leila Dargahi[2]

Received: 21 January 2015 / Accepted: 23 June 2015 / Published online: 9 July 2015


**Abstract** Receptor interacting protein 1 (RIP1) has a critical role in initiation of programmed necrosis or necroptosis. RIP1 in a close collaboration with RIP3 not only mediates necroptosis but also is involved in apoptosis and inflammatory signaling. However, the interpretation of the distinct function of RIP1 and RIP3 is complicated. Herein, we demonstrated that RIP1 inhibition in the context of LPS-induced neuroinflammation decreases RIP3 expression. Concomitant administration of Nec-1, specific inhibitor of RIP1, with LPS also attenuated the activating effect of RIP3 on metabolic enzymes, glutamate-ammonia ligase and glutamate dehydrogenase as bioenergetic determinants, in hippocampal and cortical cells. RIP1 inhibition possessed an anti-inflammatory effect and improved the antioxidant capacity against LPS. Interestingly, and opposed to some reports that necroptosis inhibition sensitizes cells to apoptosis, our results showed that RIP1 inhibition attenuates apoptotic cell death in response to LPS. The survival of neuronal function was also confirmed by measuring spontaneous alternations of rats in Y-maze. In conclusion, effects of RIP1 inhibition on RIP3 and cell death provide new approaches to ameliorate neuroinflammation and relative disorders.

**Keywords** RIP1 · RIP3 · Metabolism · Apoptosis · Neuroinflammation · Memory

✉ Leila Dargahi
l.dargahi@sbmu.ac.ir

[1] Neuroscience Research Center, Shahid Beheshti University of Medical Sciences, Tehran, Iran

[2] NeuroBiology Research Center, Shahid Beheshti University of Medical Sciences, Tehran, Iran

## Introduction

Neuroinflammation plays a critical role in the pathogenesis and progression of neurodegenerative disorders which are characterized by progressive dysfunction and loss of specific neural pathways (Hou et al. 2014). Hippocampal formation and prefrontal cortex involved in cognitive processes particularly in memory performance are assumed to be among the most vulnerable locations in a neuroinflammatory context (Niranjan 2013).

Although inducers of neuroinflammation vary in a disease-specific manner, there is a striking convergence in underlying mechanisms that result in the production of neurotoxic mediators and contribute to a variety of cell death modes (Tricarico et al. 2013). Activation of Toll-like receptors (TLRs) by host-derived molecules, as well as exogenous ligands is among the initial steps in activation of immune cell responses, a variety of downstream inflammatory cascades and production of pro-inflammatory cytokines into the surrounding areas. Of particular importance in neuroinflammation, soluble tumor necrosis factor-α (TNF-α) as a pleiotropic cytokine plays a role in cell survival and death. The binding of TNF-α to its receptor tumor necrosis factor receptor-1 (TNFR1) can alternatively induce survival or cell death through the formation of two sequential complexes. Complex I eventually dissociates from the receptor and promotes the formation of cytosolic complex II or death-inducing signaling complex (DISC). Complex II formation depends on unubiquitinated receptor interacting protein 1 (RIP1) and RIP3 as scaffolds and recruits procaspase-8 which is autoproteolytically cleaved and activated. Activation of caspase-8 and subsequent activation of executioner caspases cause apoptosis (Declercq et al. 2009; Fricker et al. 2013). Inadequate inhibitory proteolytic processing of RIP1 and RIP3 by caspase-8, as an autoregulatory mechanism, stabilizes RIP1–RIP3 interaction in a complex

named necroptosome and induces their kinase activities (Cabal-Hierro and Lazo, 2012). RIP1–RIP3 necroptosome formation activates glycolysis and glutaminolysis-enhancing bioenergetics, decreases adenosine triphosphate (ATP) levels, increases the production of reactive oxygen species (ROS) by mitochondria, and triggers lipid peroxidation. Disintegration of mitochondrial, lysosomal, and plasma membranes finally promotes the morphological features of necrosis in cells (Vandenabeele et al., 2010).

Revelation of necroptosis or programmed/regulated necrosis, as a form of cell death mediated by death receptors signaling, implicated in a wide range of pathological conditions has provided a new potential approach to inhibit neurodegeneration and neuroinflammation. Among the regulators of necroptosis, RIP1 plays a crucial role in activation of RIP3 and other downstream mediators (Guire et al. 2011) and has attracted increasing interest in the field of neuroprotection. However, the question is that how inhibition of RIP1 can be effective in the alleviation of neuroinflammatory process because it has been demonstrated that RIP3 can mediate necroptosis independent of RIP1 (Kim and Li 2013), may induce apoptosis, and can directly promote pro-inflammatory cytokine production (Khan et al. 2014). Another point is that whether RIP1 inhibition affects the apoptosis. RIP1 is a main component of DISC (Cabal-Hierro and Lazo 2012) and inhibition of RIP1 may potentiate the apoptotic pathway.

This study aimed to elucidate the effects of RIP1 inhibition on apoptosis as well as RIP3 downstream signaling elements and outcomes including glutamate-ammonia ligase (GLUL) and glutamate dehydrogenase 1 (GLUD) activity as bioenergetic determinants, antioxidant defense, and inflammatory mediators. All the molecular analyses were performed in the hippocampus and frontal cortex and accompanied with the behavioral test of spatial memory formation.

## Materials and Methods

### Materials

All materials and reagents used in this study were from Sigma–Aldrich (St. Louis, MO, USA) except those mentioned in the following text. Antibodies directed against TNF-α, RIP1, caspase-8, Bax, Bcl2, caspase-3, β-actin, and secondary antibody were obtained from Cell Signaling Technology (Beverly, MA, USA). Cyclooxygenase-2 (COX-2) antibody was obtained from ABR—Affinity BioReagents (Pierce Biotechnology, Rockford, IL). Interleukin-1β (IL-1β) and RIP3 antibodies were purchased from Santa Cruz Biotechnology (Dallas, TX, USA). Electrochemiluminescence (ECL) kit was provided from Amersham Bioscience (Piscataway, USA). Polyvinylidene fluoride (PVDF) membrane was from Millipore (Billerica, MA, USA).

### Animals

Male Wister rats (250–280 g) were housed in standard cages under controlled temperature (22 ± 2 °C), humidity, and a 12-h light/dark cycle (light on 07:00–19:00), with food and water provided ad libitum. Experimental procedure was approved by the Ethics Committee of Shahid Beheshti University of Medical Sciences in accordance with international guidelines that were confirmed by the National Institutes of Health Publication (No. 80-23, revised 1996). All efforts were made to minimize animal suffering and to reduce the number of animals used.

### Experimental Design

Animals were divided into four groups. First group received intracerebroventricular injections of 1 μl dimethylsulfoxide (DMSO) and 3 μl normal saline, with few minutes interval. Second group received 1 μl DMSO and 15 μg LPS (*E.coli* 055:B55, Sigma, USA) dissolved in 3 μl sterile saline (Gong et al. 2011; Iwai et al. 2008; Omidbakhsh et al. 2014). Rats in third group received 1 μl of Nec-1 10 μM (dissolved in DMSO) and 3 μl saline. Last group received Nec-1 and LPS co-treatment. In the next step, animals were divided into two main experimental groups of molecular and behavioral assessments. For molecular assessments, animals ($n$ = 8 per group) were sacrificed 8 h after treatments, and for behavioral studies ($n$ = 8 per group), spontaneous alternation was evaluated by Y-maze at the day 3 after treatments (based on our unpublished data).

### Stereotaxic Surgery and Microinjections

The animals were anesthetized with intraperitoneal injection of 0.2 ml mixture of ketamine hydrochloride (80 mg/kg) and xylazine (10 mg/kg). They were then implanted with guide cannula just above the right cerebral ventricle with stereotaxic coordinate of AP −0.5 mm, L +1.5 mm, and DV 3 mm (from the skull surface) according to the rat brain atlas of Paxinos and Watson (2007). After 8 days recovery, all microinjections were performed slowly over a period of 60 s using a Hamilton syringe connected to the injection needle.

### Tissue Collection

For molecular assessments, rats were divided into two subgroups. In the first subgroup, animals were sacrificed by $CO_2$ asphyxiation and decapitated ($n$ = 4 per group). Brain tissues were immediately excised and rinsed in ice-cold phosphate-buffered saline (PBS). The hippocampi and frontal cortices

were isolated on ice, snap frozen in liquid nitrogen, and then stored at −80 °C. In another subgroup, animals were perfused transcardially with PBS (pH 7.4), followed by 4 % paraformaldehyde in 0.1 M phosphate buffer (pH 7.4) under deep anesthesia ($n$ = 4 per group). The whole brains were then removed and post fixed in 4 % paraformaldehyde for 24 h and subsequently embedded in paraffin for histopathological studies and sectioned at a thickness of 5 μm.

### Preparation of Total Protein Extracts

The isolated tissues were homogenized in protein extraction buffer containing protease inhibitor cocktail and then centrifuged at 3000 rpm at 4 °C (Niimura et al. 2006). Protein content was determined according to the Bradford's method using bovine serum albumin as a reference standard (Bradford, 1976).

### Western Blotting

Equal amounts of each sample (60 μg) were loaded on SDS-PAGE and transferred to PVDF membrane. Subsequently, membranes were blocked by non-fat dry milk-TBST solution (2 %) and probed with specific primary antibodies overnight at 4 °C. After washing, membranes were incubated for 90 min at room temperature with horseradish peroxidase-conjugated secondary antibody. Immunoreactive polypeptides were detected by chemiluminescence using ECL kit reagents. Finally, quantification of results was performed by scan of X-ray films and densitometric analysis by ImageJ software.

### Glutamate-Ammonia Ligase Activity Assay

Activity of glutamine synthetase in hippocampus and frontal cortex was measured according to Kingdon et al. method (1968). Fifty microgram of each sample was mixed with the reaction cocktail containing 100 mM imidazole HCl buffer, 3 M sodium glutamate solution, 250 mM adenosine 5′s-triphosphate solution (ATP), 900 mM $MgCl_2$, 1 M KCl, 1.2 M $NH_4Cl$. Final concentrations of the components in the assay were as follows: 33 mM phospho(enol)pyrovate solution, 12.8 mM β-Nicotinamide adenine dinucleotide solution (β-NADH), and pyruvate kinase/lactic dehydrogenase enzyme solution. Condition of the reaction mixtures was constant (T = 37 °C and pH 7.1); finally, the absorbance of samples was recorded at 340 nm with respect to the blank solution.

### Glutamate dehydrogenase 1 Activity Measurement

GLUD activity was determined using a spectrophotometric assay, based on oxidation of the reduced co-enzyme NADH (Doherty, 1970). Reaction mixture contained 1 M potassium phosphate buffer pH 7, 0.5 mg/ml NADH, 1 M $NH_4Cl$, 0.1 M 2-Oxo-glutarate, and 200 μg protein of hippocampi and frontal cortices homogenized tissues. Lastly, the absorbance of samples was recorded at 340 nm.

### Measurement of Lipid Peroxidation

Malondialdehyde (MDA) levels were measured by the double heating method (Draper and Hadley, 1990). Based on this method, generation of the purple color by the reaction of thiobarbituric acid (TBA) with MDA is measured spectrophotometrically. Briefly, 200 μg of total protein of hippocampus or frontal cortex homogenate were mixed with 2.5 ml of tricholoroacetic acid (TCA, 10 % $w/v$) solution and then were boiled for 15 min in a water bath. After cooling to the room temperature, the samples were centrifuged at 3000 rpm for 10 min. Next, 2 ml of each sample was homogenized and tissue transferred to a test tube containing 1 ml of TBA solution (0.67 % $w/v$). Then, each tube was placed in boiling water for 15 min. After cooling to room temperature, the absorbance was measured at 532 nm with respect to the blank solution.

### Determination of Superoxide Dismutase Activity

Superoxide dismutase (SOD) activity was measured according to the method of Kakkar et al. (1984). Briefly, homogenized tissues were added to assay mixture including 0.052 M sodium pyrophosphate buffer pH 8.3, 186 μM phenazinemethosulphate, and 300 μM nitrobluetetrazolium. Reaction was initiated by adding 780 μM NADH and stopped by the addition of glacial acetic acid. Intensity of color was measured spectrophotometrically at 560 nm.

### Measurement of Catalase Activity

Catalase activity was measured based on the method described by Aebi (1984). Briefly, 60 μg of total protein of each homogenized tissue sample was added to $H_2O_2$ (0.01 M). Decomposition of $H_2O_2$ by the activity of catalase was monitored at 240 nm spectrophotometrically.

### Measurement of Reduced Glutathione

Reduced glutathione level was determined according to the method of Ellman (1959). Sixty microgram of total protein was added to Ellman's reagent containing 19.8 mg of dithionitrobenzoic acid (DTNB) in 100 ml of 0.1 % sodium nitrate and phosphate buffer (0.2 M, pH 8.0). The absorbance was determined at 412 nm.

### Terminal-Transferase dUTP Nick-End Labeling Staining

The terminal-transferase dUTP nick-end labeling (TUNEL) method was performed using a TUNEL assay kit (Chemicon Millipore, Temecula, CA, USA) to detect apoptotic cells in rat hippocampi. In short, coronal sections were dewaxed and then hydrated. Hydrogen peroxide 3 % was used for blocking the endogenous peroxidase activity for 3–5 min at room temperature. The sections were washed with PBS and digested for 15 min with 20 μg/ml proteinase K at room temperature. Then, tissues were incubated with 50 μl TUNEL reaction mixture for 60 min at 37 °C and further incubation with 50 μl converter-POD for 30 min at 37 °C. After rinsing with PBS, sections were incubated with 50 μl substrate solution diaminobenzidine (DAB) for 4 min at 15–25 °C and washing with PBS. Then, sections were dehydrated and cover-slipped for analysis under light microscopy. Negative controls were achieved by the omission of enzyme solution.

### Immunofluorescence

The prepared coronal sections of hippocampi were blocked with goat serum and incubated with RIP3-specific antibody (1:250 dilution) overnight at 4 °C followed by fluorescent secondary antibody Alexis Fluor 488-conjugated anti-rabbit IgG (1:150, Molecular Probes, Invitrogen, CA). Data analysis was conducted using a fluorescence microscope (OlympusIX71, Japan).

### Spontaneous Alternation Y-Maze Test

Immediate working memory performance was assessed by recording spontaneous alternation behavior during a single session in a symmetrical Y-maze apparatus as described previously (Kimura et al. 2010; Ohno et al. 2004). The test is based on the tendency of rodents to enter an arm of a Y-maze that was not explored in the

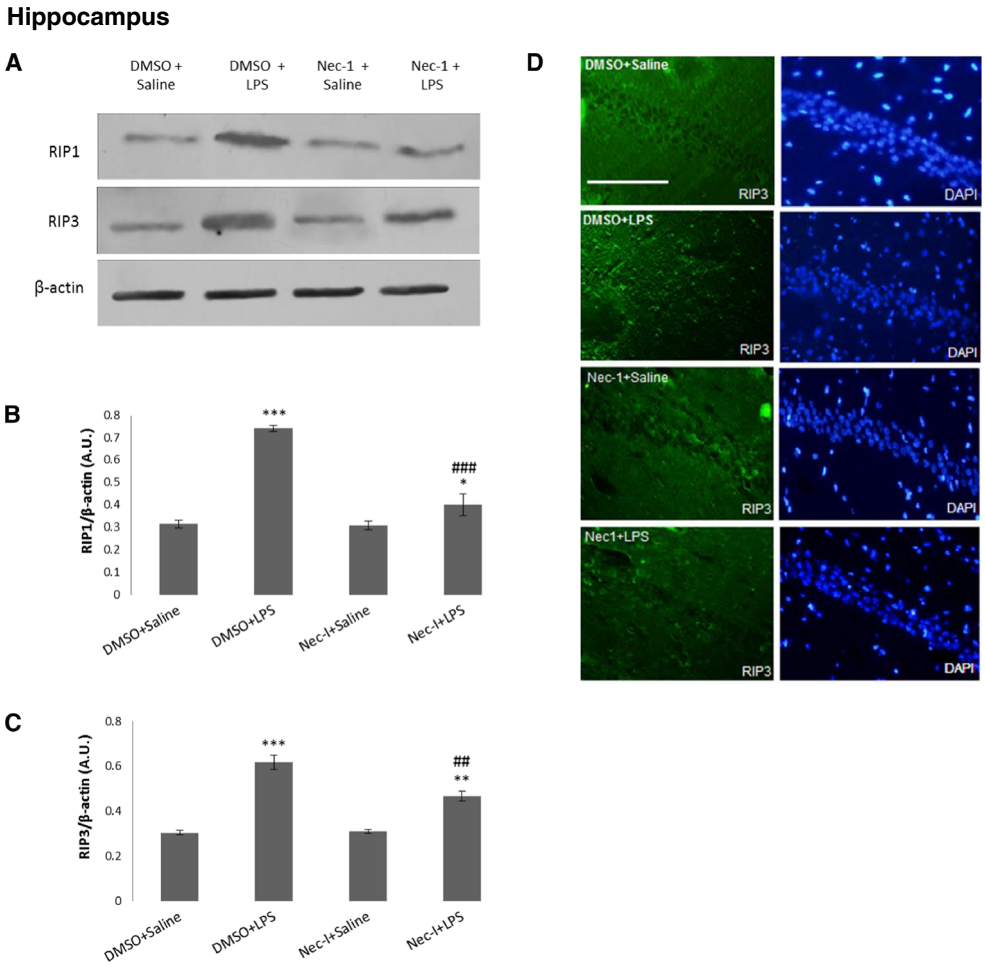


**Fig. 1** Co-administration of Nec-1 with LPS (i.c.v.) significantly reduced the expression of RIP1 and RIP3. Representative immunoblots of RIP1 and RIP3 in the hippocampus (**a**) and frontal cortex (**e**). RIP3 immunofluorescence staining in the hippocampal CA1 region. *Bar* = 50 μm (**d**). The quantitative densitometric data of Western blots (**b**, **c**, **f**, **g**) represented as relative density against β-actin. Data are mean ± SEM ($n$ = 4 for each group).*$p < 0.05$, **$p < 0.01$, ***$p < 0.001$ vs. DMSO + saline group and $^{\#\#}p < 0.01$, $^{\#\#\#}p < 0.001$ vs. DMSO + LPS group

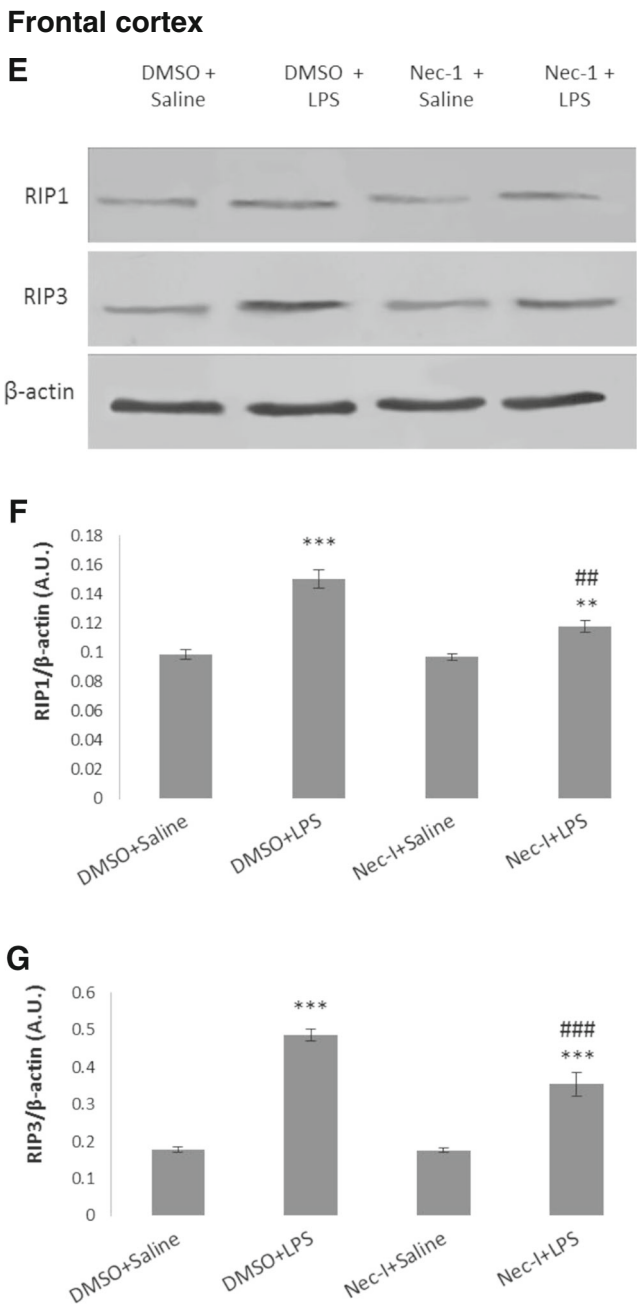


**Fig. 1** (continued)

last two choices. Each rat was placed in the center of the Y-maze and allowed to explore freely through the maze during an 8-min session. The sequence and total number of arms entered were recorded visually. Arm entry was considered to be complete when the hind paws of the rat had been completely placed in the arm. Alternation was defined as successive entries into the three arms in a triple set without repetition. Percentage of alternation is calculated by following formula: ((number of alternation)/(total number of arm entries − 2)) × 100.

### Data Analysis

All data are represented as the mean ± SEM. Comparison between groups was made by one-way analysis of variance (ANOVA) followed by a Tukey post hoc test to analyze the difference among groups. The statistical significances were achieved when $p < 0.05$.

## Results

### Effects of RIP1 Inhibition on RIP3 Expression in Hippocampus and Frontal Cortex Following LPS Injection

Our data showed that LPS significantly increases necroptosis-regulatory factors, RIP1 and RIP3, in target tissues and therefore results in necroptotic cell death. Here, Nec-1 efficiency as a specific RIP1 inhibitor was studied in a preliminary dose–response experiment, and the best inhibitory effect on RIP1 in LPS-induced neuroinflammatory state was found at the concentration of 10 μM (data not shown). As shown in Fig. 1a–c, co-administration of Nec-1 with LPS reduced RIP1 along with RIP3 in hippocampus ($p < 0.001$ and $p < 0.01$, respectively) compared to the group that received vehicle instead of Nec-1. Consistent with Western blot findings, our immunofluorescence data also showed an increased expression of RIP3 in LPS-injected group and a profound reduction of RIP3 in the group that received Nec-1 before LPS (Fig. 1d). Induction of necroptosis by intracerebroventricular injection of LPS was also observed in frontal cortex, and co-administration of Nec-1 decreased the levels of RIP1 and RIP3 ($p < 0.01$ and $p < 0.001$, respectively), in comparison to LPS-treated group (Fig. 1e–g).

### Effects of RIP1 Inhibition on GLUL and GLUD Enzymes Activity in Hippocampus and Frontal Cortex Following LPS Injection

As shown in Fig. 2a–d, LPS injection enhanced GLUL and GLUD activity in the hippocampus and frontal cortex. Surprisingly, this increased activity of enzymes GLUL and GLUD was significantly alleviated by Nec-1 co-administration with LPS. GLUL activity was decreased by 29 % and 44 % in hippocampus and frontal cortex respectively, in groups that received Nec-1 and LPS compared to the group that received DMSO and LPS. Nec-1 also attenuated hippocampal GLUD activity by 56 % and cortical GLUD activity by 23 % in the LPS-injected rats compared to the DMSO and LPS co-administrated animals.

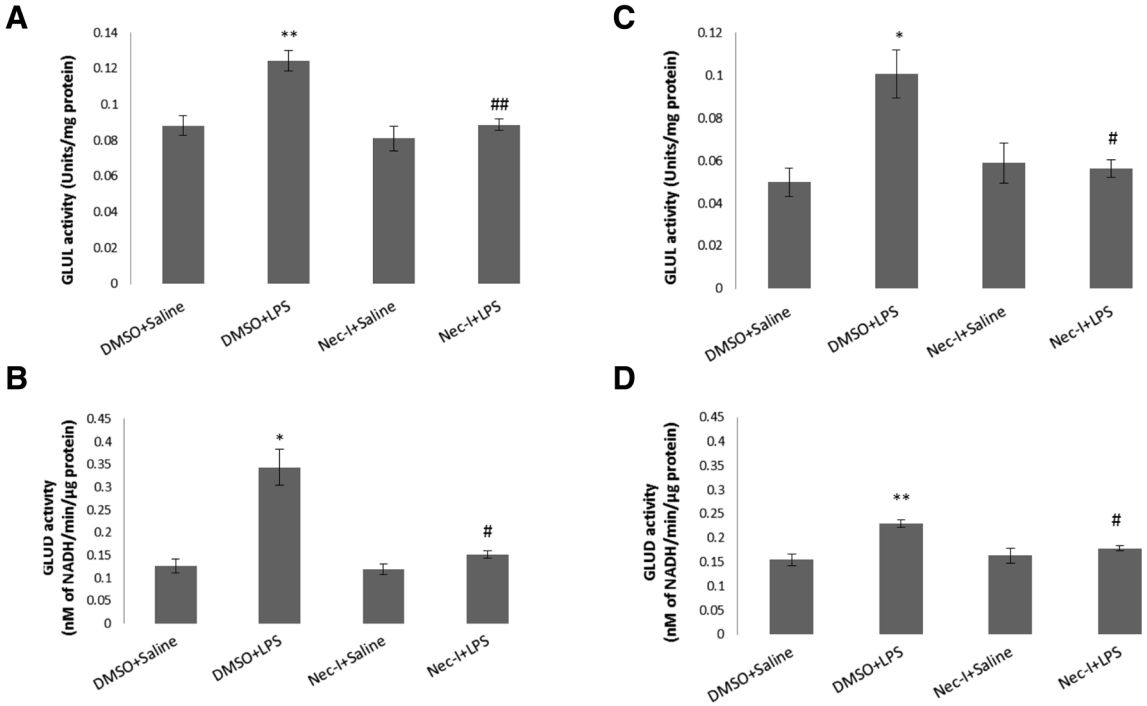


**Fig. 2** RIP1 inhibition affected the activity of two enzymes catalyzing glutamate–glutamine interconversion. Analysis of the activity of GLUL and GLUD in the hippocampus (**a**, **b**) and frontal cortex (**c**, **d**) showed a significant increase in LPS-injected rats and decrease in those co-treated with Nec-1. Data are mean ± SEM ($n$ = 4 for each group).*$p < 0.05$, **$p < 0.01$ vs. DMSO + saline group and $^{\#}p < 0.05$, $^{\#\#}p < 0.01$ vs. DMSO + LPS group

### Effects of RIP1 Inhibition on Bax/Bcl2 Ratio, Cleaved Caspase-3, and Cleaved Caspase-8 in the Hippocampus and Frontal Cortex Following LPS Injection

Efficiency of RIP1 inhibition for downregulation of apoptosis pathway is controversial. In order to reveal the effect of RIP1 inhibition on procedure of apoptosis pathway in designed groups, we measured protein levels of main proapoptotic factors; Bax, cleaved caspase-3 and cleaved caspase-8, and anti-apoptotic factor Bcl2 by Western blot. Morphological evaluation was also performed by TUNEL assay in the hippocampus. As shown in Fig. 3a–d, intracerebroventricular injection of LPS increased Bax/Bcl2 ratio, cleavage of caspase-3, and cleavage of caspase-8 ($p < 0.001$). However, co-injection of Nec-1 with LPS prevented from the increase of apoptotic factors compared to the animals that received DMSO and LPS ($p < 0.001$). Histological analysis also confirmed less TUNEL-positive (apoptotic) cells in the sections of rats co-treated with Nec-1 and LPS compared to the group that received DMSO and LPS (Fig. 3e). It should be mentioned that while biochemical assays were performed on whole hippocampus, morphological data referred to specific subdivision, i.e., CA1 area. Also, as shown in Fig. 3f–i, Bax/Bcl2 ratio, cleaved caspase-3, and cleaved caspase-8 in the frontal cortex of Nec-1 and LPS co-administrated rats were also significantly decreased compared to the animals that received DMSO and LPS ($p < 0.001$).

### Effects of RIP1 Inhibition on Oxidative Stress Relative Enzymes Activity, GSH Content, and MDA Concentration

As was expected, LPS injection provoked an oxidative stress manifested by decreased activity of oxidative stress-related enzymes SOD and catalase, reduced concentration of glutathione (GSH), and increased levels of MDA in the hippocampus and frontal cortex of rats. Augmentation of SOD and catalase activity, increase in GSH content, and decrease in MDA concentration in Nec-1 co-administrated group revealed the protective effect of RIP1 inhibition against LPS-induced oxidative stress (Table 1).

**Fig. 3** RIP1 inhibition prevented the activation of apoptotic pathways in response to LPS. Representative immunoblots of Bax, Bcl-2, cleaved caspase 3, and cleaved caspase-8 in the hippocampus (**a**) and frontal cortex (**f**). TUNEL staining of apoptotic cells in the hippocampal CA1 region. *Bar* = 10 μm (**e**). The quantitative densitometric data of Western blots (**b–d** and **g–i**) represented as relative density against β-actin. Data are mean ± SEM ($n$ = 4 for each group).*$p < 0.05$, **$p < 0.01$, ***$p < 0.001$ vs. DMSO + saline group and $^{\#\#\#}p < 0.001$ vs. DMSO + LPS group

## Hippocampus

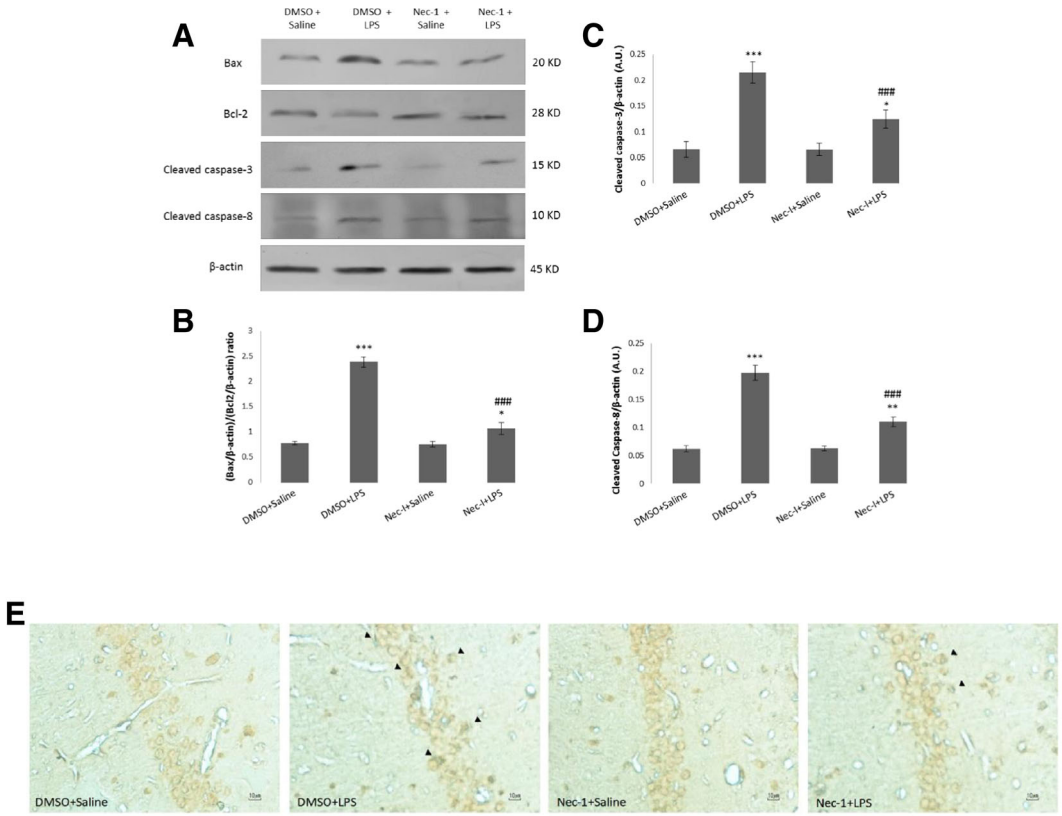





## Frontal cortex

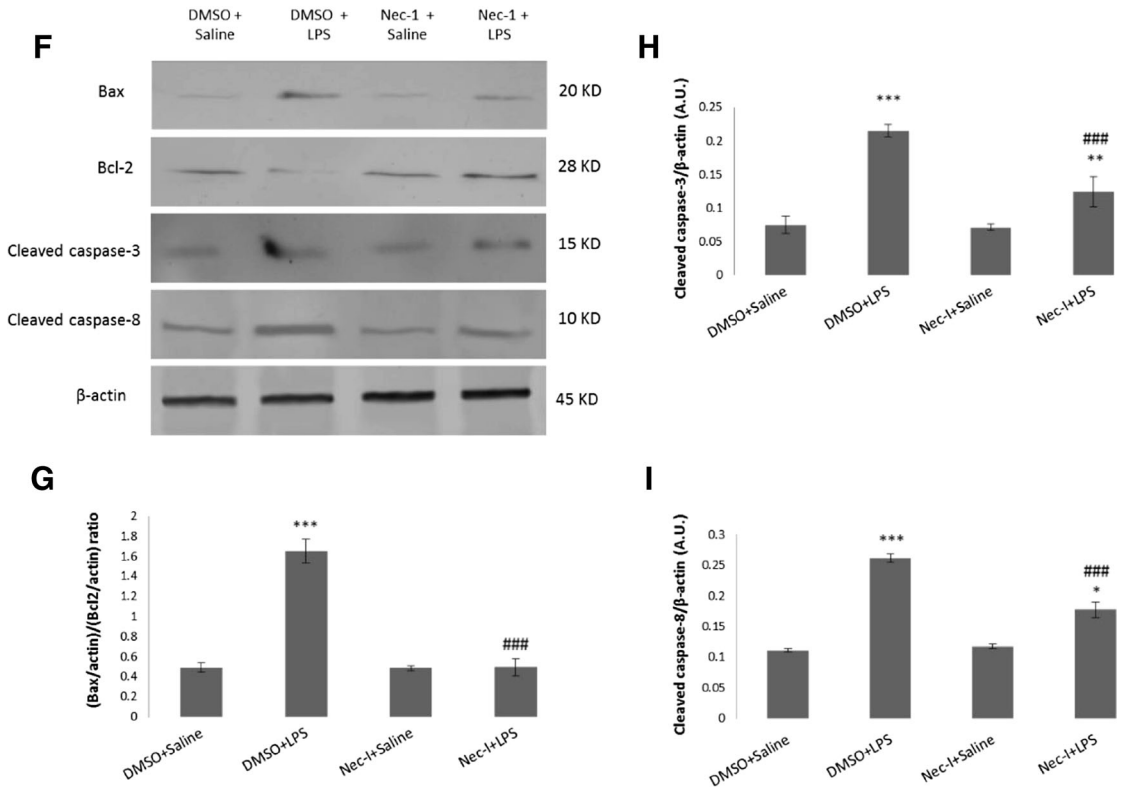

**Table 1** The effect of RIP1 inhibition on SOD and catalase activity and GSH and MDA contents in hippocampal and frontal cortex tissues of rats

| Tissues | Groups | SOD (U/mg protein) | Catalase (nmol/mg protein) | GSH (U/mg protein) | MDA (nmol/mg protein) |
|---|---|---|---|---|---|
| Hippocampus | DMSO + saline | 76.54 ± 0.64 | 2.3 ± 0.26 | 12.3 ± 0.12 | 1.8 ± 0.07 |
| | DMSO + LPS | 70.14 ± 1.33** | 0.75 ± 0.21* | 11.79 ± 0.06* | 2.07 ± 0.04* |
| | Nec-1 + saline | 77.58 ± 1.132 | 2.19 ± 0.34 | 11.74 ± 0.1 | 1.78 ± 0.02 |
| | Nec-1 + LPS | 79.33 ± 1.32$^{\#\#\#}$ | 1.93 ± 0.16$^{\#}$ | 11.75 ± 0.07$^{\#}$ | 1.74 ± 0.02$^{\#}$ |
| Frontal cortex | DMSO + saline | 86.54 ± 1.04 | 0.52 ± 0.03 | 13.50 ± 0.18 | 1.71 ± 0.14 |
| | DMSO + LPS | 78.14 ± 0.35*** | 0.12 ± 0.08** | 12.24 ± 0.12* | 2.03 ± 0.06* |
| | Nec-1 + saline | 82.79 ± 0.41 | 0.47 ± 0.05 | 13.41 ± 0.45 | 1.75 ± 0.05 |
| | Nec-1 + LPS | 82.42 ± 1.5$^{\#\#}$ | 0.48 ± 0.03$^{\#\#}$ | 13.41 ± 0.4$^{\#}$ | 1.62 ± 0.004$^{\#\#}$ |

Each point shows the mean ± SEM; number per group, 4

*Compared to DMSO + saline group, $^{\#}$ compared to DMSO + LPS group. * or $^{\#}$ $p < 0.05$; ** or $^{\#\#}$ $p < 0.01$; *** or $^{\#\#\#}$ $p < 0.001$

### Effects of RIP1 Inhibition on Inflammatory Mediators in the Hippocampus and Frontal Cortex of LPS-Injected Rats

To confirm the neuroinflammatory effect of LPS and the potential anti-inflammatory role of RIP1 inhibition, we measured the levels of key inflammatory mediators, TNF-α, IL-1β, and COX-2, in the hippocampus and frontal cortex of animals in experimental groups. As shown in Fig. 4, LPS significantly increased the expression of TNF-α, IL-1β, and COX-2 ($p < 0.001$), in the hippocampus and frontal cortex and this effect was hampered by RIP1 inhibition. As shown in Fig. 4a–d, Nec-1 co-administration with LPS decreased the level of TNF-α, IL-1β, and COX-2 in the hippocampus compared to the group that received DMSO and LPS ($p < 0.001$). In the same way, the levels of TNF-α and COX-2 ($p < 0.001$) and IL-1β ($p < 0.01$) decreased in the frontal cortex of Nec-1- and LPS-administered rats compared to animals that received DMSO and LPS (Fig. 4e–h).

### Effect of RIP1 Inhibition on LPS-Induced Spatial Memory Impairment

As shown in Fig. 5, our results in Y-maze test showed that LPS significantly decreases the percent of spontaneous alternation ($p < 0.001$), while RIP1 inhibition protects against impairment of spatial short-term memory induced by LPS ($p < 0.05$). LPS and other treatments had no effect on the total number of arm entries.

## Discussion

In this study, RIP1 inhibition in an inflammatory context influenced RIP3 downstream signaling elements and outcomes including GLUL and GLUD activity, antioxidant defense, apoptosis pathway and inflammatory hallmarks, and also restored short-term spatial memory formation.

Regarding RIP1-independent effects of RIP3 on cell death (Kaiser et al. 2011), the question was that whether RIP1 inhibition can influence RIP3 and its downstream events. In answering this question, we first measured RIP3 and its downstream events like GLUL and GLUD enzyme activity and the anti-oxidative defense against LPS-induced toxicity and showed that in parallel to RIP1, RIP3 expression and function also increases in response to LPS. Interestingly, this RIP3 increment was reversed by Nec-1-mediated-RIP1 inhibition, and this is while Takahashi and his colleagues have proved that Nec-1 and its analogues have no direct inhibitory effects on RIP3 activity (Takahashi et al. 2012).

A crucial function of RIP3 signaling is to promote cell survival by increasing cellular energy level. In fact, RIP3 governs the cell's metabolic state. RIP3 directly interacts with GLUL and GLUD1. Both GLUL and GLUD have vital functions for the use of glutamate or glutamine as substrates for ATP production in oxidative phosphorylation. GLUL catalyzes the condensation of glutamate (Glu) and ammonia to form glutamine (Gln). Gln transfers into the mitochondria and is converted to Glu to function as an energy substrate. Then, GLUD converts Glu to α-ketoglutarate. RIP3 activity is necessary to enhance the activity of these enzymes in cellular and animal models. (Zhang et al. 2009; Declercq et al. 2009). However, little is known about the regulation of GLUL and GLUD in necroptotic cells. Our study showed that inhibition of RIP1 attenuates RIP3 and its downstream elements including GLUL and GLUD enzyme activities. Actually, this decrement in RIP3 level and GLUL and GLUD activity through RIP1 inhibition finally leads to attenuation of cell metabolism rate; and therefore, there is a direct link between necroptosis and metabolism rate of the cell.

Activated RIP3 enhances the energy metabolism which results in ROS accumulation (Zhang et al. 2009). To evaluate the inhibitory effects of RIP1

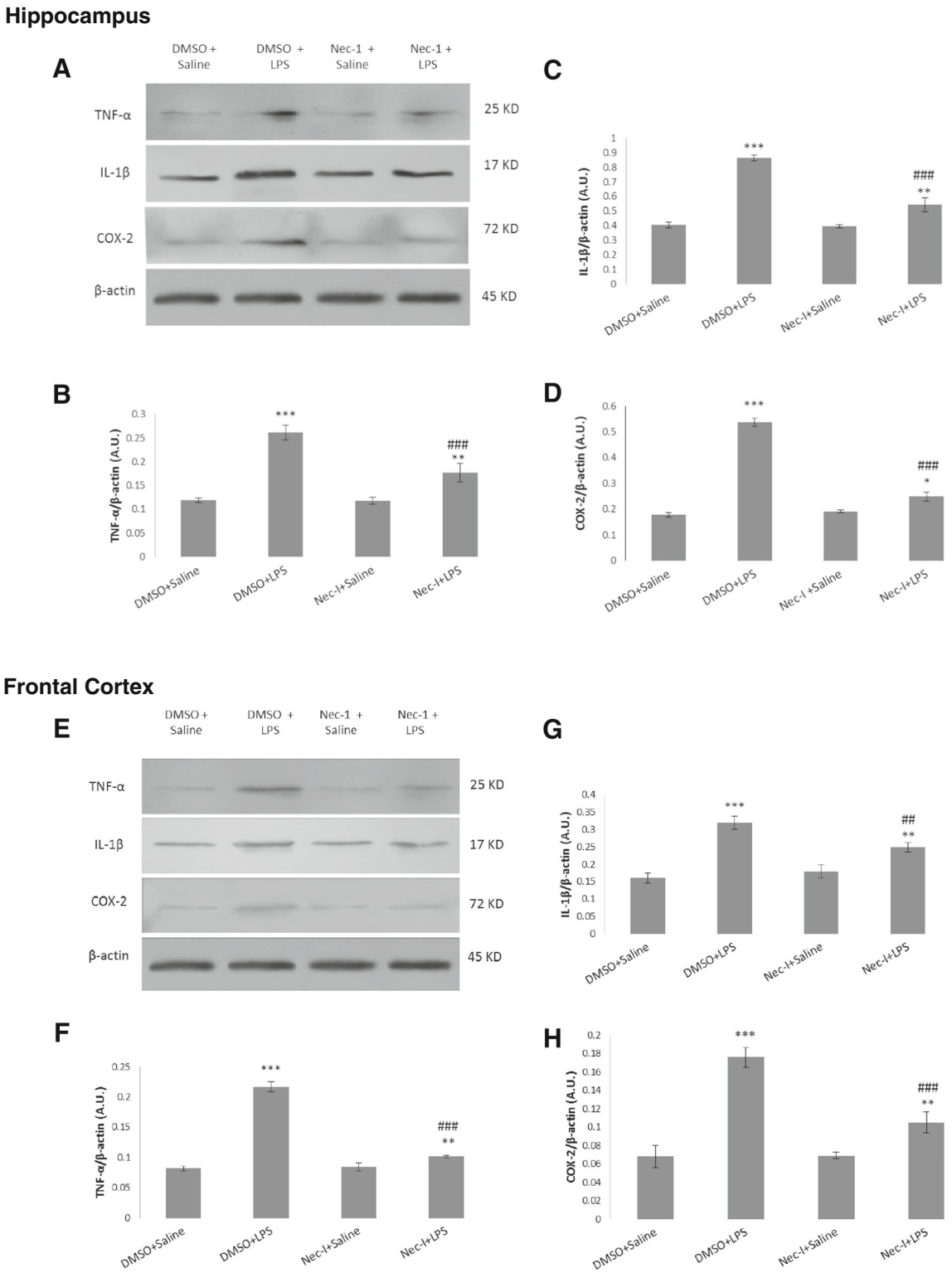


**Fig. 4** RIP1 inhibition reduced the expression of inflammatory mediators in response to LPS. Representative immunoblots of TNF-α, IL-1β, and COX-2 in the hippocampus (**a**) and frontal cortex (**e**). The quantitative densitometric data of Western blots (**b–d** and **f–h**) represented as relative density against β-actin. Data are mean ± SEM ($n = 4$ for each group).*$p < 0.05$, **$p < 0.01$, ***$p < 0.001$ vs. DMSO + saline group and $^{\#\#}p < 0.01$, $^{\#\#\#}p < 0.001$ vs. DMSO + LPS group

inhibition on RIP3-induced impairment of antioxidant defense, we measured SOD and catalase activity and content of GSH and MDA. Our results showed that RIP1 inhibition improves antioxidant protection against

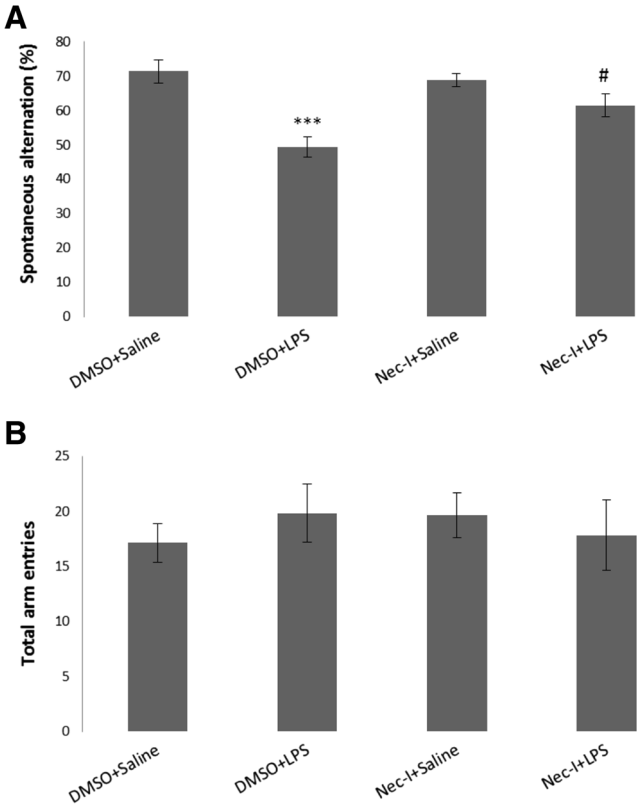


**Fig. 5** RIP1 inhibition protected against LPS-induced memory impairment. Spatial short-term memory was studied 3 days after LPS injection using Y-maze. Co-administration of Nec-1 with LPS significantly improved spontaneous alternation percentage (**a**). No significant differences in total arm entries among groups (**b**). Data are mean ± SEM ($n = 8$ for each group). ***$p < 0.001$ vs. DMSO + saline group and $^{\#}p < 0.05$ vs. DMSO + LPS group

LPS-induced toxicity. In agreement to these data, it has been shown that Nec-1 decreases GSH depletion following glutamate treatment (Xu et al. 2007). Nec-1 administration also reduces the expression of some genes related to oxidative stress in myocardial ischemic reperfusion injury model (Oerlemans et al. 2012), enhances the activity of SOD, and reduces MDA concentration in a model of spinal cord injury (Wang et al. 2014).

RIP1 inhibition has proved potential to inhibit necroptotic cell death (Degterev et al. 2005); however, the possibility of the conversion of cell death to an apoptotic state is a contentious zone in the crossroad of apoptosis and necroptosis. While some reports show that Nec-1 has no effects on apoptosis (Degterev et al. 2005; You et al. 2008; Rosenbaum et al. 2010), some others have demonstrated that inhibition of necroptosis may sensitize the cells to apoptosis (Han et al. 2012; Han et al. 2009; Northington et al. 2011). Interestingly, in a rat model of traumatic spinal cord injury, it has been shown that Nec-1 inhibits apoptosis in parallel to necroptosis inhibition (Wang et al. 2014). Though there is no doubt that these controversies can be attributed to different contexts of studies, our results showed that RIP1 inhibition reduces the cleaved caspase-8 as a key molecule in the death receptor-mediated apoptosis. Investigating the role of caspase-8 in different kinds of cell death, Kikuchi et al. have reported that caspase-8 knockdown cells not only undergo necroptosis but also endure apoptosis and autophagic cell death. The occurrence of apoptosis in caspase-8-deficient cells can be assigned to the accumulation of ROS and activation of intrinsic pathway; however, Kikuchi et al. have demonstrated that both RIP1 and RIP3 are key factors in mediating cell death in these conditions. They showed that RIP1 inhibition as well as RIP3 gene knockdown are both effective in attenuating all kinds of cell death (Kikuchi et al. 2012). Accordingly and as described, our results further to the decrease in cleaved caspase-8 showed the downregulation of Bax/Bcl2 ratio and apoptosis executioner enzyme caspase-3 in response to inhibition of RIP1 in neuroinflammatory context induced by LPS. Similarly, in a mouse model of intracerebral hemorrhage, RIP1 inhibition attenuates apoptotic pathway and exerts neuroprotective effects by decreasing caspase-3 cleavage and augmentation of Bcl2 upregulation (Chang et al. 2014).

Administration of LPS results in robust glial activation and induces brain inflammation. Activated microglia are the main source of inflammatory cytokines, such as IL-1β and TNF-α (Miwa et al. 2011; Wyss-Coray and Rogers 2012). Our data demonstrated that RIP1 inhibition by Nec-1 could alleviate pro-inflammatory cytokines production, including TNF-α, IL-1β, and also COX-2 enzyme in the hippocampus and frontal cortex. It sounds that one of the possible mechanisms through which LPS increases the production of inflammatory mediators is activation of RIP1. As the others have also shown, inhibition of RIP1 can reduce inflammation in CNS (Northington et al. 2011; Wang et al. 2014; You et al. 2008) and other tissues like the liver (Zhou et al. 2013) and heart (Oerlemans et al. 2012). The anti-inflammatory effects of RIP1 inhibition may be attributed to the reduction of necroptotic cell death and the downstream events in hippocampal and cortical cells.

Balanced energy metabolism, enhanced antioxidant capacity, reduced cell death, and less cytokine production following RIP1 inhibition can improve functional survival of hippocampal and cortical neurons in LPS-induced neuroinflammatiory events. The survival of neuronal function was confirmed in this study by measuring spontaneous alternations of rats in Y-maze.

Evidence suggests that spontaneous alternation in Y-maze is a measure of spatial working memory (Richman et al. 1987) and neural activities in the septohippocampal pathway are critical circuits for this type of memory (Givens 1995). It

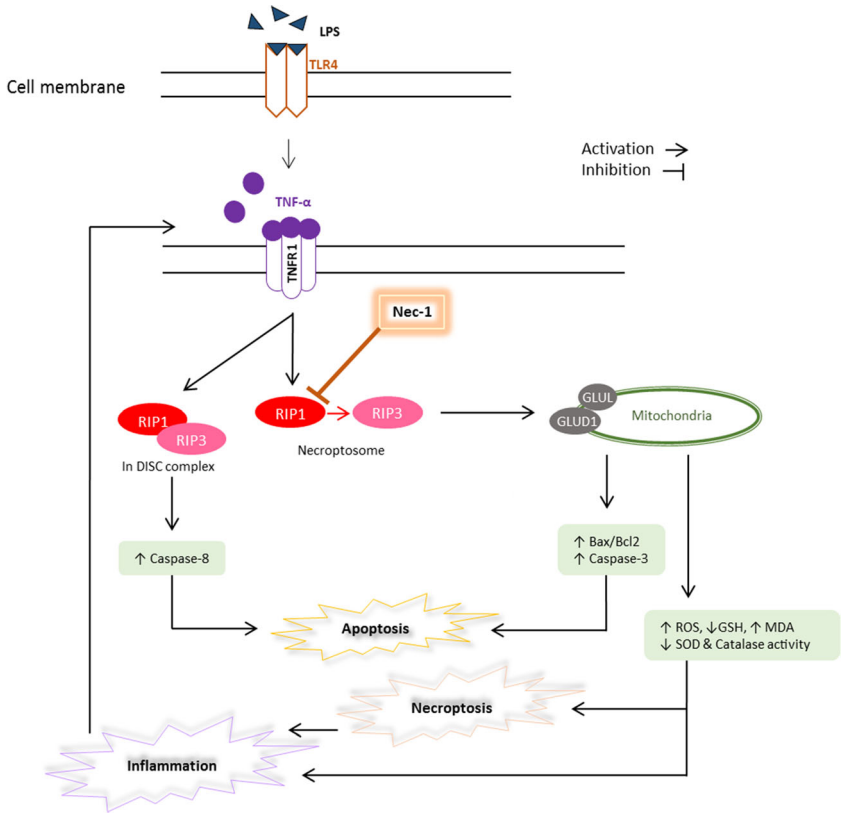


**Fig. 6** Schematic diagram of possible downstream events of RIP1 inhibition

has been reportedly shown that LPS-induced neuroinflammation impairs learning and memory in different tasks like Y-maze and morris water maze (Hou et al. 2014). Inhibition of RIP1 is demonstrated to potentially improve mice learning and memory functions and cognitive performance due to upregulation of mGluR2 and mGluR5 in cerebral cortical tissue in an aluminum-induced neurotoxicity model (Qinli et al. 2013). Protective effect of RIP1 inhibition on learning and memory performance has been also observed in a mouse model of traumatic brain injury by administration of Nec-1 (You et al. 2008).

In summary, we demonstrated that RIP1 inhibition attenuates RIP3 expression and function, reserves cell metabolism rate, enhances the power of anti-oxidative defense, prevents hippocampal and cortical cell death, reduces inflammatory mediators, and finally protects against short-term spatial memory impairment induced by LPS (Fig. 6). Although Nec-1 is a selective inhibitor of RIP1 and therefore inhibits necroptosis, the broad range of observed beneficial effect can be also attributed to an indirect effect on RIP3 and disruption of the vicious cycle of oxidative stress, cell death, and inflammatory reactions. Further studies are strongly encouraged on the role of RIP1 and its potential as a therapeutic target in neurodegenerative diseases and brain injuries. Further studies are also required to discriminate other possible RIP1-independent functions of Nec-1.

**Acknowledgments** This work was carried out as part of a PhD project and financially supported by the Neuroscience Research Center, Shahid Beheshti University of Medical Sciences.

## References

Aebi H (1984) Catalase in vitro. Methods Enzymol 105:121–126

Bradford M (1976) A rapid and sensitive method for the quantitation of microgram quantities of protein utilizing the principle of protein-dye binding. Anal Biochem 72:248–254

Cabal-Hierro L, Lazo PS (2012) Signal transduction by tumor necrosis factor receptors. Cell Signal 24:1297–1305. doi:10.1016/j.cellsig.2012.02.006

Chang P, Dong W, Zhang M, et al. (2014) Anti-necroptosis chemical necrostatin-1 can also suppress apoptotic and autophagic pathway to exert neuroprotective effect in mice intracerebral hemorrhage model. J Mol Neurosci 52:242–249. doi:10.1007/s12031-013-0132-3

Declercq W, Berghe TV, Vandenabeele P (2009) Minireview RIP kinases at the crossroads of cell death and survival. Cell 8:229–232

Degterev A, Huang Z, Boyce M, et al. (2005) Chemical inhibitor of nonapoptotic cell death with therapeutic potential for ischemic brain injury. Nat Chem Biol 1:112–119. doi:10.1038/nchembio711

Doherty D (1970) l-glutamate dehydrogenases (yeast). Methods Enzymol 17:850–856

Draper HH, Hadley M (1990) Malondialdehyde determination as index of lipid peroxidation. Methods Enzymol 186:421–431

Ellman GL (1959) Tissue sulfhydryl groups. Arch Biochem Biophys 82: 70–77

Fricker M, Vilalta A, Tolkovsky AM, Brown GC (2013) Caspase inhibitors protect neurons by enabling selective necroptosis of inflamed microglia. J Biol Chem 288:9145–9152. doi:10.1074/jbc.M112.427880

Givens B (1995) Low doses of ethanol impair spatial working memory and reduce hippocampal theta activity. Alcohol Clin Exp Res 19: 763–767

Gong Q, Wanga Q, Pan L, Liu X, Xin H, Zhu Y (2011) S-propargyl-cysteine, a novel hydrogen sulfide-modulated agent, attenuates lipopolysaccharide-induced spatial learning and memory impairment: involvement of TNF signaling and NF-jB pathway in rats. Brain Behav Immun 25:110–119

Guire C, Beyaert R, Loo G (2011) Death receptor signalling in central nervous system inflammation and demyelination. Trends Neurosci 34:619–628

Han W, Xie J, Li L, Liu Z, Hu X (2009) Necrostatin-1 reverts shikonin-induced necroptosis to apoptosis. Apoptosis 14:674–686. doi:10.1007/s10495-009-0334-x

Han W, Xie J, Fang Y, Wang Z, Pan H (2012) Nec-1 enhances shikonin-induced apoptosis in leukemia cells by inhibition of RIP-1 and ERK1/2. Int J Mol Sci 13:7212–7225. doi:10.3390/ijms13067212

Hou Y, Xie G, Miao F, et al. (2014) Pterostilbene attenuates lipopolysaccharide-induced learning and memory impairment possibly via inhibiting microglia activation and protecting neuronal injury in mice. Prog Neuro-Psychopharmacol Biol Psychiatry 54:92–102. doi:10.1016/j.pnpbp.2014.03.015

Iwai T, Iinuma Y, Kodani R, Oka J (2008) Neuromedin U inhibits inflammation-mediated memory impairment and neuronal cell-death in rodents. Neurosci Res 61:113–119. doi:10.1016/j.neures.2008.01.018

Kaiser WJ, Upton JW, Long AB, et al. (2011) RIP3 mediates the embryonic lethality of caspase-8-deficient mice. Nature 471:368–372. doi:10.1038/nature09857

Kakkar P, Das B, Viswanathan PN (1984) A modified spectrophotometric assay of superoxide dismutase. Indian J Biochem Biophys 21:130–132

Khan N, Lawlor K E, Murphy J M, Vince JE (2014) More to life than death: molecular determinants of necroptotic and non-necroptotic RIP3 kinase signaling. Curr Opin Immunol 26:76-89.

Kikuchi M, Kuroki S, Kayama M, Sakaguchi S, Lee KK, Yonehara S (2012) Protease activity of procaspase-8 is essential for cell survival by inhibiting both apoptotic and nonapoptotic cell death dependent on receptor-interacting protein kinase 1 (RIP1) and RIP3. J Biol Chem 287:41165–41173

Kim SJ, Li J (2013) Caspase blockade induces RIP3-mediated programmed necrosis in toll-like receptor-activated microglia. Cell Death Dis 4:e716. doi:10.1038/cddis.2013.238

Kimura R, Devi L, Ohno M (2010) Partial reduction of BACE1 improves synaptic plasticity, recent and remote memories in Alzheimer's disease transgenic mice. J Neurochem 113:248–261. doi:10.1111/j.1471-4159.2010.06608.x

Kingdon HS, Hubbard JS, Stadtman ER (1968) Regulation of glutamine synthetase. XI The Nature and Implications of a lag Phase in the Escherichia coli Glutamine Synthetase Reaction Biochemistry 7: 2136–2142

Miwa M, Tsuboi M, Noguchi Y, Enokishima A, Nabeshima T, Hiramatsu M (2011) Effects of betaine on lipopolysaccharide-induced memory impairment in mice and the involvement of GABA transporter 2. J Neuroinflammation 8:153. doi:10.1186/1742-2094-8-153

Niimura M, Takagi N, Takagi K, et al. (2006) Prevention of apoptosis inducing factor translocation is a possible mechanism for protective effects of hepatocyte growth factor against neuronal cell death in the hippocampus after transient forebrain ischemia. J Cereb Blood Flow Metabolism 26:1354–1365

Niranjan R (2013) Molecular basis of etiological implications in Alzheimer's disease: focus on neuroinflammation. Mol Neurobiol 48:412–428. doi:10.1007/s12035-013-8428-4

Northington FJ, Chavez-Valdez R, Graham EM, Razdan S, Gauda EB, Martin LJ (2011) Necrostatin decreases oxidative damage, inflammation, and injury after neonatal HI. J Cereb Blood Flow Metab 31: 178–189. doi:10.1038/jcbfm.2010.72

Oerlemans MI, Liu J, Arslan F, Den Ouden K, Van Middelaar BJ, Doevendans PA, Sluijter JP (2012) Inhibition of RIP1-dependent necrosis prevents adverse cardiac remodeling after myocardial ischemia reperfusion in vivo. Basic Res Cardiol 107:270–278

Ohno M, Sametsky EA, Younkin LH, et al. (2004) BACE1 deficiency rescues memory deficits and cholinergic dysfunction in a mouse model of Alzheimer's disease. Neuron 41:27–33

Omidbakhsh R, Rajabli B, Nasoohi S, et al. (2014) Fingolimod affects gene expression profile associated with LPS-induced memory impairment. Exp Brain Res 232:3687–3696. doi:10.1007/s00221-014-4052-4

Paxinos G, Watson C (2007) The rat brain in stereotaxic coordinates. Elsevier Academic press, Amsterdam

Qinli Z, Meiqing L, Xia J, et al. (2013) Necrostatin-1 inhibits the degeneration of neural cells induced by aluminum exposure. Restor Neurol Neurosci 31:543–555. doi:10.3233/RNN-120304

Richman CL, Dember WN, Kim P (1987) Spontaneous alternation behavior: a review. Curr Psychol 5:385–391

Rosenbaum DM, Degterev A, David J, et al. (2010) Necroptosis, a novel form of caspase-independent cell death, contributes to neuronal damage in a retinal ischemia-reperfusion injury model. J Neurosci Res 88:1569–1576. doi:10.1002/jnr.22314

Takahashi N, Duprez L, Grootjans S, et al. (2012) Necrostatin-1 analogues : critical issues on the specificity, activity and in vivo use in experimental disease models. Cell Death Dis 3:e437–e410

Tricarico PM, Marcuzzi A, Piscianz E, Monasta L, Crovella S, Kleiner G (2013) Mevalonate kinase deficiency and neuroinflammation: balance between apoptosis and pyroptosis. Int J Mol Sci 14:23274–23288

Vandenabeele P, Galluzzi L, Vanden Berghe T, Kroemer G (2010) Molecular mechanisms of necroptosis: an ordered cellular explosion. Nat Rev Mol Cell Biol 11:700–714. doi:10.1038/nrm2970

Wang Y, Wang H, Tao Y, Zhang S, Wang J, Feng X (2014) Necroptosis inhibitor necrostatin-1 promotes cell protection and physiological function in traumatic spinal cord injury. Neuroscience 266:91–101. doi:10.1016/j.neuroscience.2014.02.007

Wyss-Coray T, Rogers J (2012) Inflammation in Alzheimer disease—a brief review of the basic science and clinical literature. Cold Spring Harb Perspect Med 2:a006346. doi:10.1101/cshperspect.a006346

Xu X, Chua CC, Kong J, Kostrzewa RM, Kumaraguru U, Hamdy RC, Chua B (2007) Necrostatin-1 protects against glutamate-induced glutathione depletion and caspase-independent cell death in HT-22 cells. J Neurochem 103:2004–2014

You Z, Savitz SI, Yang J, et al. (2008) Necrostatin-1 reduces histopathology and improves functional outcome after controlled cortical impact in mice. J Cereb Blood Flow Metab 28:1564–1573. doi:10.1038/jcbfm.2008.44

Zhang DW, Shao J, Lin J, et al. (2009) RIP3, an energy metabolism regulator that switches TNF-induced cell death from apoptosis to necrosis. Science 325:332–336. doi:10.1126/science.1172308

Zhou Y, Dai W, Lin C, et al. (2013) Protective effects of necrostatin-1 against concanavalin A-induced acute hepatic injury in mice. Mediat Inflamm 2013:706156. doi:10.1155/2013/706156